JOURNAL OF MATERIALS SCIENCE 23 (1988) 3232–3242

Surface bead formation of a mild steel by pulsed current TIG arc

T. ISHIDA
Institute for Materials Research, Tohoku University, Katahira, Sendai, Miyagi Prefecture, Japan

The influence of pulse frequency on the surface bead formation and the fusion boundary microstructure of a mild steel was investigated using a pulsed current TIG arc within low and middle frequency regions. The appearance of the beads formed on the surface shows a distinct ripple shape. However, in the middle frequency region and at faster travel speeds, humped beads are formed. The number of ripples on the surface bead increases and decreases with increasing pulsed frequency and travel speed, respectively. The bead width and depth both increase with increasing pulse frequency and travel speed. In particular, a large decrease in the melt penetration is observed at middle frequency, which is probably due to a lowering of arc gouging and a discontinuity of the bead. The minimum reduction in grain size is obtained at pulse frequencies of 2.5, 5.0, 50 and 100 Hz, which is an equiaxed structure in the fusion zone, and consists of acicular ferrite and fine pearlite in a heat-affected zone. The best bead formation occurred at pulse frequencies of 2.5 and 5.0 Hz, and a travel speed of 280 mm min^{-1}.

1. Introduction

A pulsed current arc welding was recently carried out with the intention of stabilizing the arc, achieving high quality of the weld, and producing an all-position weld, etc. This pulsed arc possesses two levels of current instead of the single level that is used conventionally. Pulsating current or pulsating arc is produced by switching between a high and a low level of current. Each pulse consists of its own wave shape, high and low pulse currents and high and low pulse times.

The effect of the wave shape of the pulse current on the appearance of the weld bead and the solidification pattern has been reported to be indicative of the marked influence it has at low frequencies, compared with the bead appearance, scalloping effect of penetration and the longitudinal microstructure with varying per cent of weld current, pulse ratio, and pulse frequency [1, 2]. Grain-size control has been shown to be possible by proper selection of pulse current parameters. Grain refinement may be attributed to a melting vibration in the partially melted heat-affected zone of the base metal and previously solidified pulses [3], multiple cycling of the fusion zone into the austenite region at a restricted travel speed [4] and a difference in the degree of constitutional supercooling at the pulse frequency of 0.5 to 10 Hz [5].

In such cases, pulsed current arc can be used in several ways to join thin and medium thickness materials, in which an intense moving action of the molten pool occurs through the pulsation of the arc. This motion of molten pool under the pulsed arc has been little investigated to date.

The present paper is concerned primarily with the characteristics of formation and morphology of the bead on the surface melting of a mild steel by a pulsed arc moving at a fixed speed, in order to improve the microstructure in the fusion zone, fusion boundary region and heat-affected zone, and also to make it easy to join dissimilar metals such as iron and copper,

TABLE I Operating parameters for the pulsed current arc process

Parameter	Values
Pulse arc type	Direct current inverter TIG
Electrode	Tungsten 2.0 mm diameter
Nozzle	Ceramic collet 2.4 mm diameter
Shielding gas	Argon at a flow of 10.0 litre min^{-1}
Pulse current, I_P (A)	250 (150)*
Base current, I_B (A)	150 (100, 200, 250, 300)*
Pulse time ratio t_p/t_B	50% I/I
Pulse frequency, f (Hz)	Low frequency region: 0.5, 1.0, 2.5, 5.0 Middle frequency region: 50, 100, 200, 500
Travel speed of torch, v (mm min^{-1})	130, 280 (200, 360, 440)*
Joint method	Upright bead-on-plate
Base metal	Mild steel: 5 mm × 40 mm × 100 mm

*Test carried out with these values according to their purpose.

0022–2461/88 $03.00 + .12

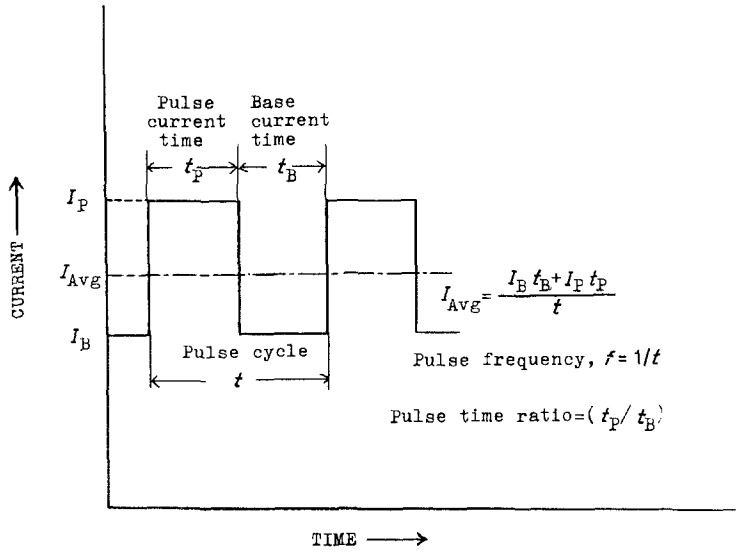

Figure 1 An idealized pulsed current waveform and associated parameters.

iron and aluminium, etc., taking full advantage of the pulsed current arc.

2. Experimental details

The material used in this investigation was a commercial grade 5 mm thick plate of a mild steel (C 0.13, Si 0.16, Mn 0.58, Ni 0.020, Cr 0.043, P 0.024, S 0.021, Al 0.027 wt %). It was cut into specimen coupons of dimensions 40 mm × 100 mm and then the areas of the specimen surface which were to be struck by the pulsed arc were ground clean using an emery belt and paper. The bead-on-plate arrangement was made using an Hitachi inverter TIG 300NP welder. The operating conditions of the pulsed current arc are listed in Table I.

Fig. 1 shows a schematic representation of an ideal pulsed current rectangular waveform involving the associated pulse parameters [6]. For this waveform, the average current, I_{Avg}, is

$$I_{Avg} = \frac{I_B t_B + I_P t_P}{t} \quad (1)$$

where I_B and I_P are the base and pulse currents, t_B and t_P their respective durations and t the time of the pulse cycle. The cycle time is

$$t = t_B + t_P \quad (2)$$

The pulse frequency, f, is the inverse of the cycle time (f, Hz)

$$f = \frac{1}{t} = \frac{1}{t_B + t_P} \quad (3)$$

The ratio of base current time divided by pulse current time is called the pulse time ratio, t_P/t_B. These pulse parameters were evaluated in terms of their influence on bead formation and the resulting microstructure.

Voltage and current waveforms during experimentation were observed and recorded using a dual channel oscilloscope used in the welding circuit shown in Fig. 2. Channel 1 of the oscilloscope was a.c. coupled across the arc to allow sufficient gain for arc transient observation. Channel 2 was a.c. coupled into the current measurement using a 50 mV–300 A shunt. Traces of arc voltage and current were stored on the oscilloscope and photographed. Typical oscilloscope traces observed under conditions of the circuit shown in Fig. 2 are in Fig. 3. The wave shapes obtained are a waveform with overshoot on both the leading and trailing edges. Overshoot often accompanies a pulse with a rapid rise time. Furthermore, in order to obtain a more clearer waveform, it is convenient to use the inductive measurement method in which three windings encircling the cable inductor near the positive iron table are connected to the oscilloscope. The arc current waveform obtained by using the inductive measurement method is shown in Fig. 4, indicating a waveform with an overshoot.

Under such experimental conditions of arc pulsation, surface bead formation was induced on mild steel materials by the moving pulsed arc. The number of ripples produced on mild steel surface bead were determined and the specimens were then sectioned transversely and longitudinally to examine the

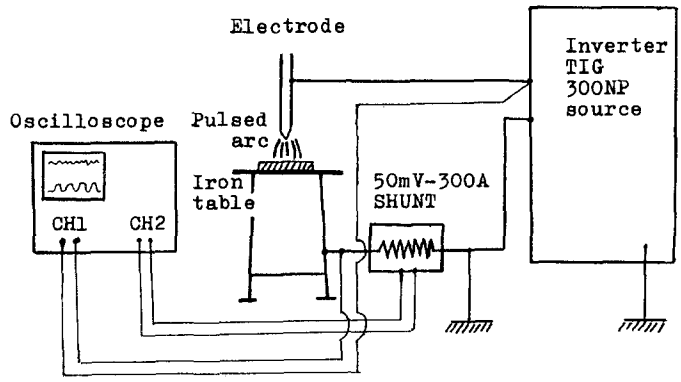

Figure 2 A diagram of the electrical circuit for the measurement of arc current and voltage waveforms.

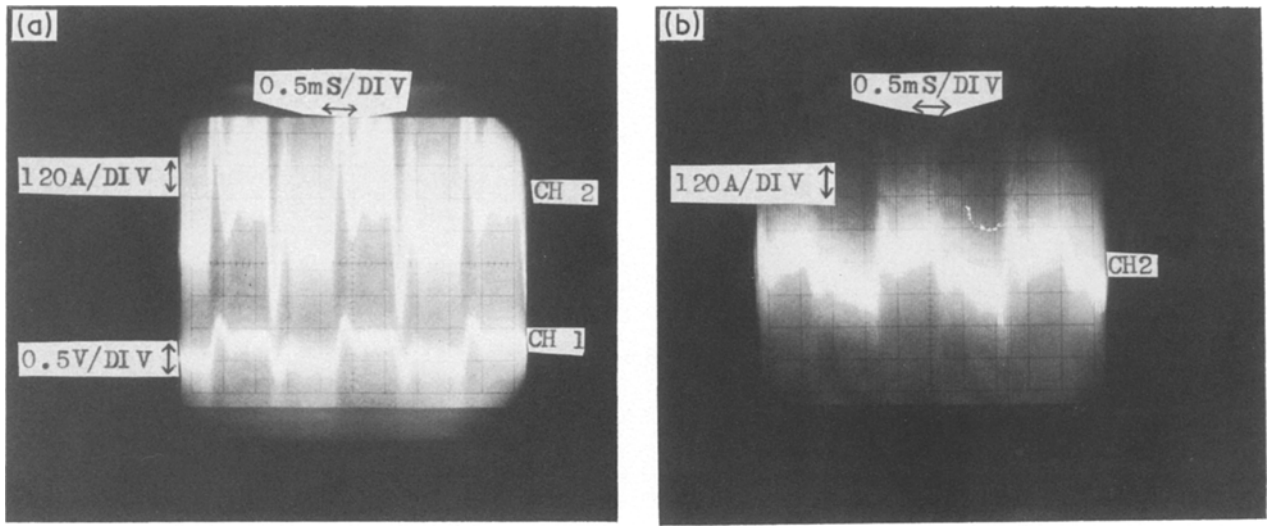

Figure 3 Oscilloscope traces of the wave shapes of pulsed current arc and arc voltage, measured using the electrical circuit of Fig. 2. Pulse current 150 A, base current 50 A, pulse frequency 500 Hz, pulse time ratio 50%. (a) Current (CH2) and voltage (CH1) waveforms. (b) Current waveform (CH2).

microstructures of the fusion zone, fusion boundary region and heat-affected zone.

3. Results and discussion

3.1. Formation of a surface bead

Figs 5 and 6 indicate the effect of base current and travel speed of the torch on the surface bead width of a mild steel for a given pulse current. Fig. 5 shows the increase in melt-zone width with increasing base current, the relationship is approximately linear, whereas a decrease in melt-zone width with increasing travel speed of the torch is seen in Fig. 6. This increase in melt-zone width is due to the influence of heat-input increment on increasing the base current and decreasing the travel speed.

Figs 7 and 8 show the appearance of a surface bead of the mild steel which were made on the plate by impact of the pulse arc for a given torch travel speed in the ranges of the low and middle frequencies. For the low frequency region, the surface bead appearance has a distinct ripple wave shape (Figs 7a to d and 8a to d), while for the middle frequency region with lower travel speed, the appearance only has a slight ripple wave shape (Figs. 7e to h). For the middle frequency range and a high travel speed, the formation of imperfect bead shape is observed (Figs 8a to h). With low and middle pulse frequencies and slower travel speed, the surface bead appearance has a regular ripple shape, but with high pulse frequency and faster travel speeds, an irregular-shaped surface bead forms. The formation of this imperfect bead is thought to be due to the very violent motion of the molten metal beneath the pulsed arc with a high pulse frequency and a fast travel speed.

Figs 9 and 10 show the influence of pulse frequency on the ripple formation on the mild steel surface bead. At low frequencies the number of ripples increases parabolically with increasing pulse frequency and decreases with increasing travel speed (Fig. 9). As the frequency becomes higher, the number of ripples seems to remain constant, but at high travel speed, the number of ripples cannot be counted (Fig. 10). At low frequencies, very regular ripples are seen which correspond to the pulsing of the current. At high frequencies as the travel speed becomes fast, there is very little evidence of ripples corresponding to the pulsing arc. At travel speeds above some critical value, the surface of the molten metal is considered to be considerably disordered by the high pulsed current arc.

The effects of the pulse frequency on the melt-zone width and depth are shown in Figs 11 and 12, respectively. The bead width decreases gradually with increasing pulse frequency. In particular, in the middle frequency region and at a travel speed of 280 mm min^{-1}, the magnitude of the decrease is a little large (Fig. 11). The melt penetration decreases with increasing pulse frequency, except in the low frequency region and at a travel speed of 130 mm min^{-1} (Fig. 12). A large decrease in the penetration is observed at middle frequencies. Both the width and depth decrease

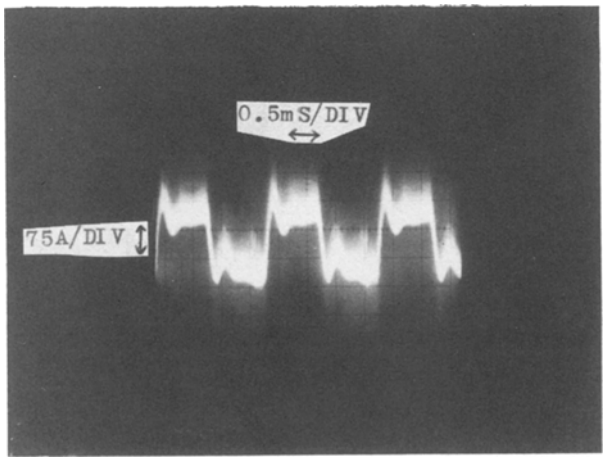

Figure 4 Arc current waveform observed using the inductive measurement method. Pulse current 200 A, base current 50 A, pulse frequency 500 Hz, pulse time ratio 50%.

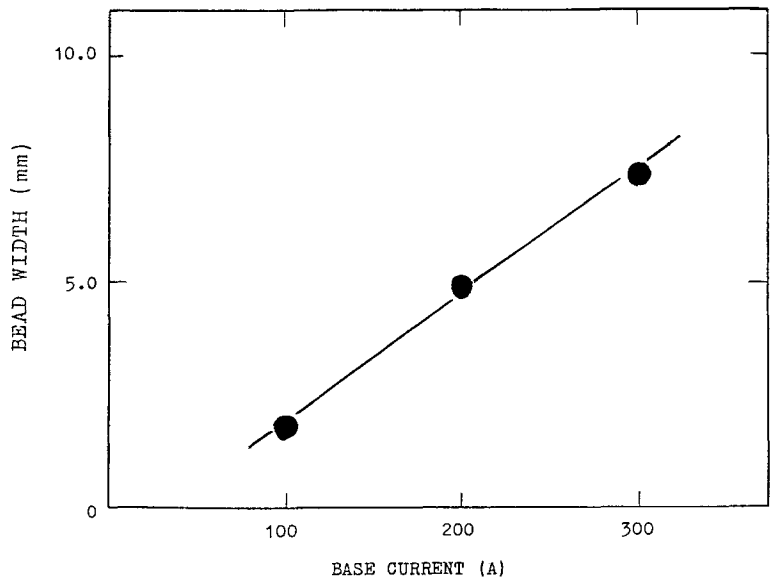

Figure 5 Relationship between bead width and base current under the pulsed current arc. Pulse current 150 A, pulse time ratio 50%, pulse frequency 500 Hz, travel speed 280 mm min^{-1}.

with increasing travel speed. This decrease of the penetration at high pulse frequency is probably the result of a lowering of the arc gouging and formation of a discontinuity on the bead under the pulsed current arc.

At a low pulse frequency of some Hertz, melting and solidifying actions on the surface portion of the material, depending on the long pulse period, are duplicated a number of times, the resultant ripples corresponding to the pulse current. Accordingly, relatively smooth surface beads are formed. On the other hand, as the pulse frequency becomes higher, the variation of the time on heat input, independent of the configuration and size of melt penetration, gives a vigorous fluctuation in the molten pool below the pulsed arc. Further, as a travel speed becomes fast, discontinuous beads arise on the material surface from the turbulence in the molten pool beneath the pulsed current arc. Accordingly, a humped bead is formed on the melted surface portion of the mild steel. Thus, at high frequency and fast travel speed, occurrence of an abnormal bead is caused by the violent fluctuation and discontinuity of molten metal not corresponding to the pulse period [2].

3.2. Transverse microstructure

A metallographic study of the fusion zone (FZ), fusion line (FL) and head-affected zone (HAZ) was performed to determine the effect of pulse frequency on the microstructure. Fig. 13 shows the microstructures of fusion zone, fusion-boundary region and heat-affected zone in transverse section, produced by pulsed current arc at pulse frequencies of 0.5 Hz and 50 Hz. In spite of a low frequency of 0.5 Hz, the microstructure of the fusion zone in Fig. 13a consists of relatively fine primary ferrite and pearlite present, which is probably due to the influence of a precipitation by rapid cooling in the central part of the fusion zone. However, the ferrite in the fusion zone and HAZ near the fusion line becomes comparatively large as shown in Fig. 13b. On the other hand, as pulse frequency is increased, the microstructure of the fusion zone and HAZ becomes finer at 50 Hz as shown in Fig. 13c and d. Thus, it is noted that a significant decrease in grain size was obtained by increasing pulse frequency. This reduction in grain size is probably caused by ease of granule formation to allow separation from the melt of branches and trunks of the dendrite [5].

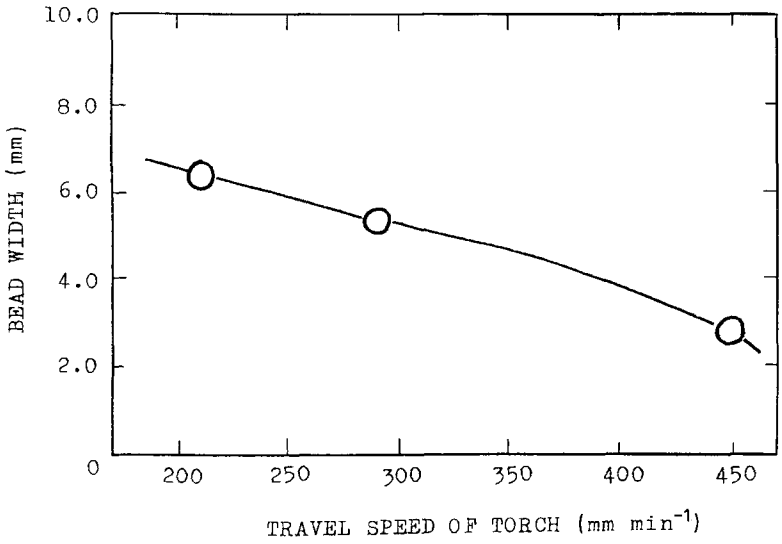

Figure 6 Relationship between bead width and travel speed of the torch under the pulsed current arc. Pulse current 250 A, base current 150 A, pulse time ratio 50%, pulse frequency 500 Hz.

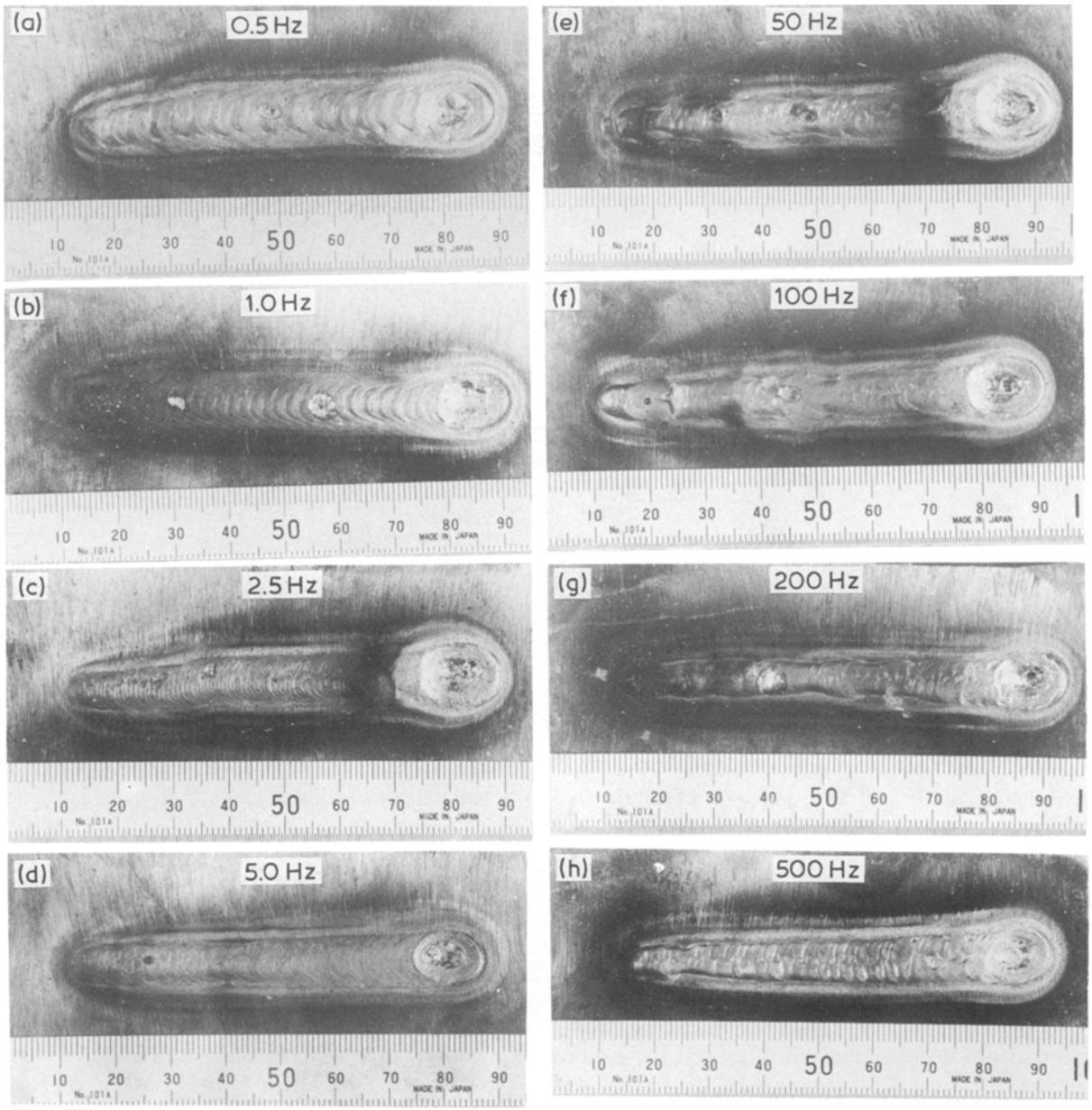

Figure 7 Surface bead appearance of mild steel formed by a pulsed current arc moving at a speed of 130 mm min^{-1} at low frequencies of 0.5 to 5.0 Hz and middle frequencies of 50 to 500 Hz. Pulse current 250 A, base current 150 A, pulse time ratio 50%. (a) 0.5 Hz, (b) 1.0 Hz, (c) 2.5 Hz, (d) 5.0 Hz, (e) 50 Hz, (f) 100 Hz, (g) 200 Hz, (h) 500 Hz.

3.3. Longitudinal macro- and micro-structures

The macro longitudinal cross-sections with changing the travel speeds (130 and 280 mm min^{-1}) at a low pulse frequency of 0.5Hz, are shown in Fig.14. At a travel speed of 280 mm min^{-1}, the induced solidification pattern corresponding to the pulse frequency can readily be seen, indicating a wavy pattern (Fig. 14a). The wavy solidification pattern becomes more noticeable with faster travel speeds and lower pulse frequencies. This wavy pattern is similar to the scalloping effect of penetration which becomes more prominent with faster wave shape current decay time, higher pulse time ratio, lower pulse frequency and faster travel speeds [1]. At a travel speed of 130 mm min^{-1}, the solidification pattern has become a straight line and no wave is present (Fig. 14b). The disappearance of the scalloping effect appears to be due to a continuous and steady penetration pattern.

Figs 15 and 16 show the longitudinal microstructures of mild steel beads with various pulse frequencies for travel speeds of 130 and 280 mm min^{-1}, respectively, while keeping the other pulse parameters constant. The effect of pulse frequency on the grain size was investigated quantitatively from this longitudinal solidification microstructure.

For a travel speed of 130 mm min^{-1}, at low frequencies of 2.5 Hz and 5.0 Hz, and middle frequencies of 50 and 100 Hz, a fine microstructure is obtained in the fusion zone and the HAZ, in which, in particular, a gradual change from columnar to equiaxed structure occurs in the fusion zone (Fig. 15a to f). For middle frequencies of 200 and 500 Hz, the matrix structure of the fusion zone is columnar and the grain size in the

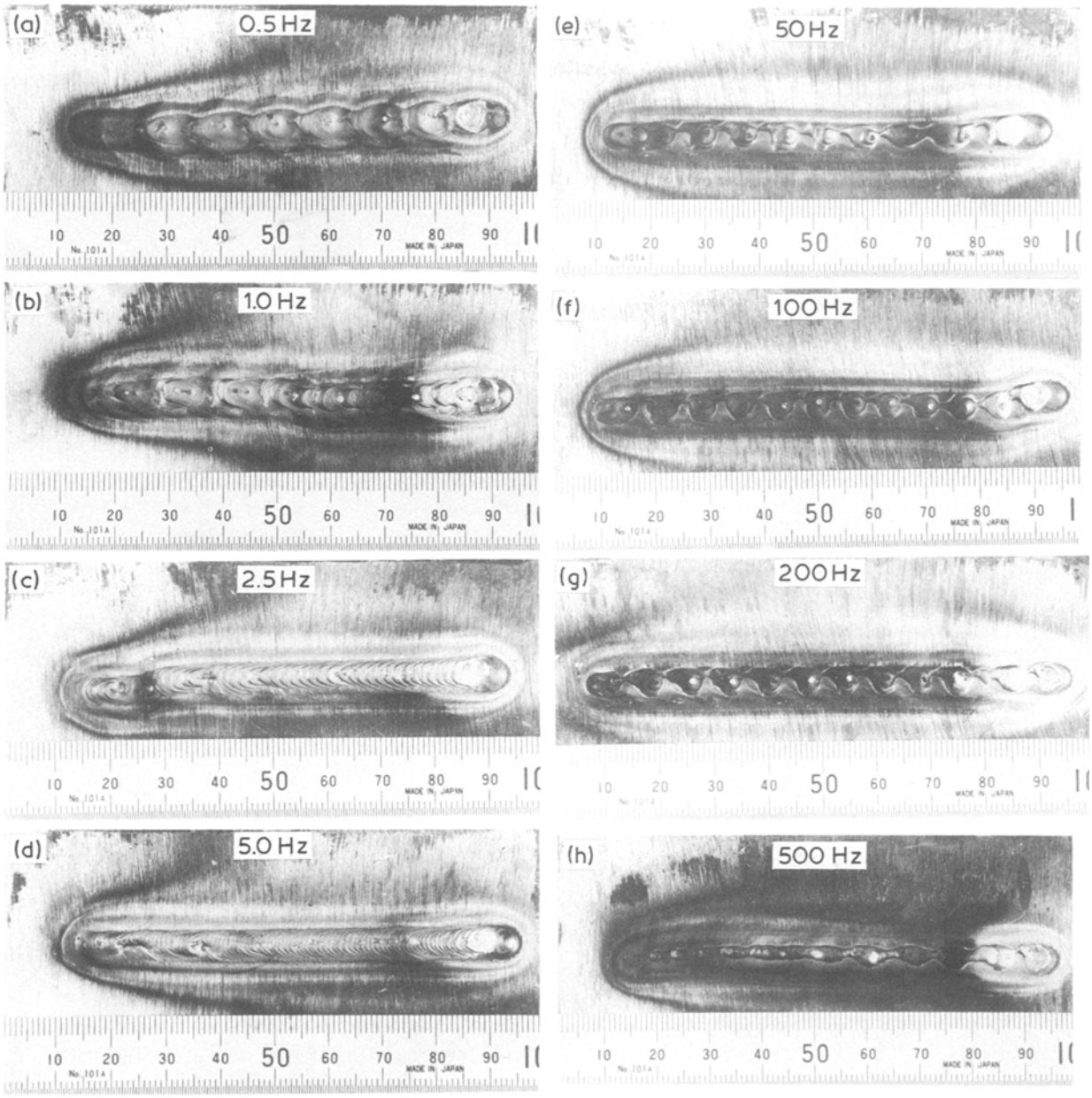

Figure 8 Surface bead appearance of mild steel formed by a pulsed current arc moving at a speed of 280 mm min^{-1} at low frequencies of 0.5 to 5.0 Hz and middle frequencies of 50 to 500 Hz. Pulse current 250 A, base current 150 A, pulse time ratio 50%. (a) 0.5 Hz, (b) 1.0 Hz, (c) 2.5 Hz, (d) 5.0 Hz, (e) 50 Hz, (f) 100 Hz, (g) 200 Hz, (h) 500 Hz.

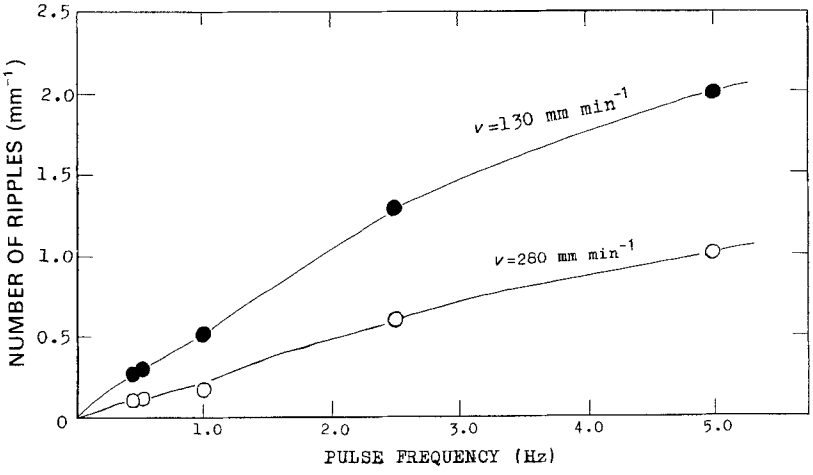

Figure 9 Number of ripples produced on the mild steel surface bead with low frequencies. Pulse current 250 A, base current 150 A, pulse time ratio 50%, argon gas 10.0 litre min^{-1}, base metal – mild steel.

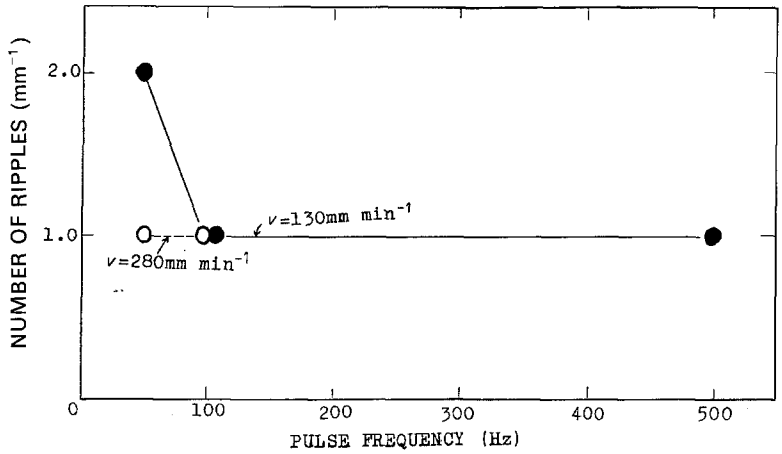

Figure 10 Number of ripples produced on the mild steel surface bead with middle frequencies. Pulse current 250 A, base current 150 A, pulse time ratio 50%, argon gas 10.0 litre min^{-1}.

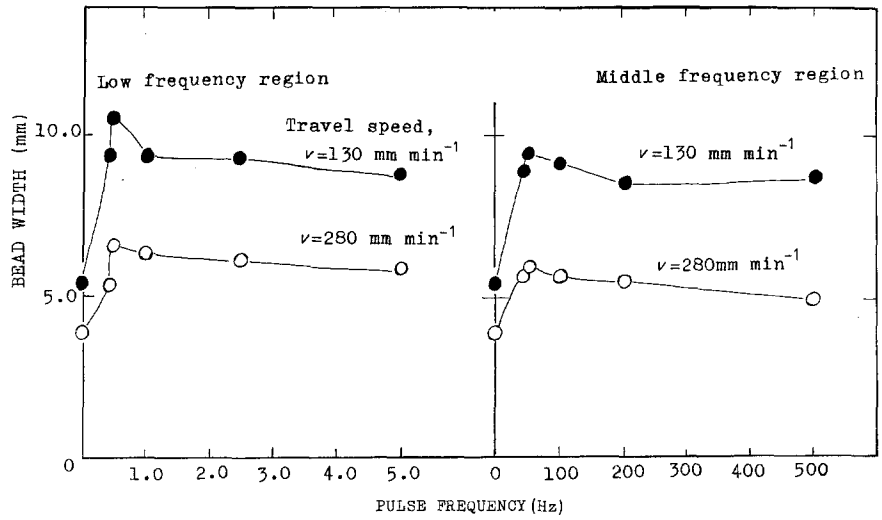

Figure 11 Influence of pulse frequency on surface melt width of the mild steel under pulsed current arc. Pulsed current 250 A, base current 150 A, pulse time ratio 50%, argon gas 10.0 litre min^{-1}.

fusion and heat-affected zones becomes adversely large (Fig. 15g and h).

On the other hand, when the travel speed is 280 mm min^{-1}, at low frequencies of 2.5 and 5.0 Hz and middle frequencies of 50 and 100 Hz, a finer microstructure is obtained in the fusion zone and the HAZ, in which pearlites become very fine and primary ferrites are equiaxed (Fig. 16a to f). As the pulse frequency becomes 200 and 500 Hz, an increase of the grain size is observed in the fusion zone and the HAZ (Fig. 16g and h), which shows the changes to columnar structure in the fusion zone and ferrite side plate in the HAZ. An increase in pulse frequency from 2.5 to 100 Hz decreases the grain size in the fusion and heat-affected zones, while increased travel speed enhances the reduction in grain size. Reduction in grain size in this pulse frequency range is probably due to the granular appearance causing a melting separation of

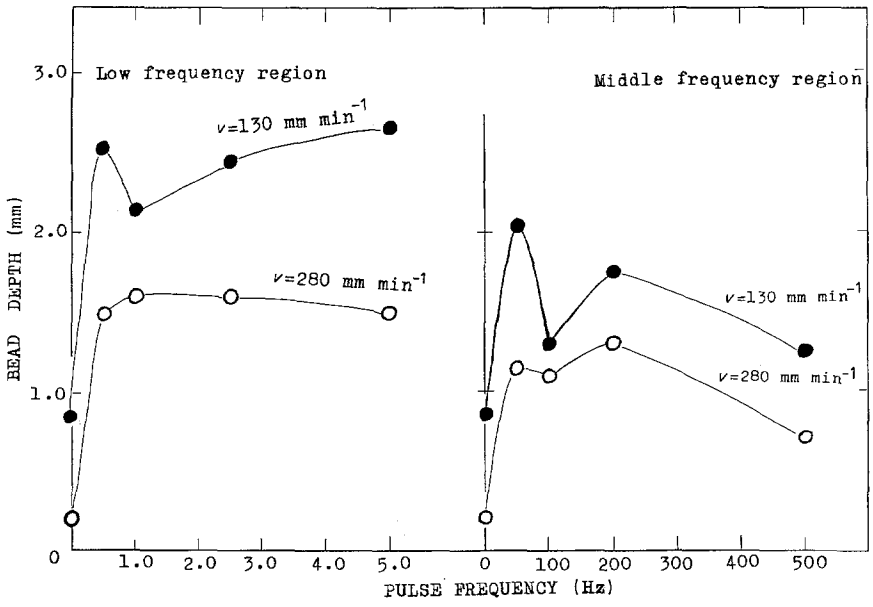

Figure 12 Influence of pulse frequency on melt penetration of the mild steel under pulsed current arc. Pulse current 250 A, base current 150 A, pulse time ratio 50%, argon gas 10.0 litre min^{-1}.

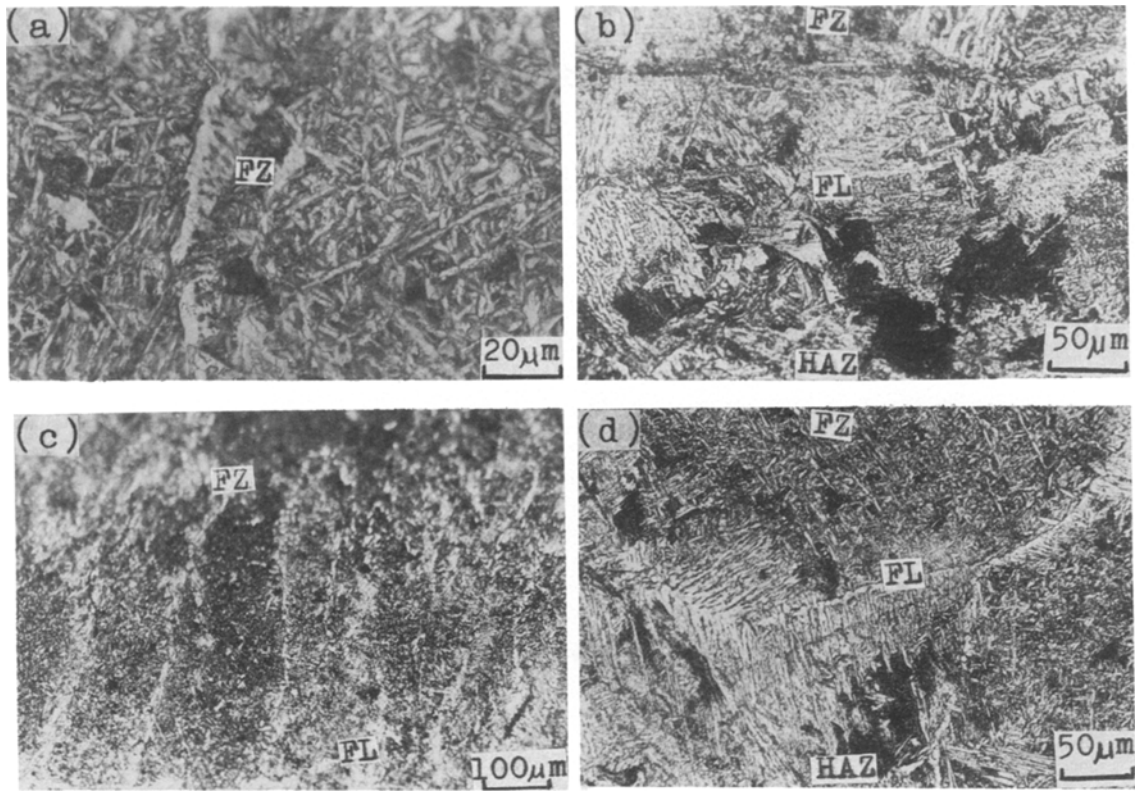

Figure 13 Transverse microstructures of mild steel produced by pulsed current arc at pulse frequencies of 0.5 and 50 Hz. Pulse current 250 A, base current 150 A, travel speed 130 mm min^{-1}, pulse time ratio 50%. (a) Fusion zone, frequency 0.5 Hz; (b) fusion-boundary region, frequency 0.5 Hz; (c) fusion zone, frequency 50 Hz; (d) fusion-boundary region, frequency 50 Hz.

the dendrites [5]. However, above 200 Hz, the grain size becomes adversely larger. The increase in grain size in the high pulse frequency may be attributed to the formation of a columnar structure by a complete continuity of epitaxial growth having a narrow pulse interval.

3.4. Morphology of bead formation

The characteristics of bead formation of mild steel on the bead appearance and the microstructure of the fusion-boundary region observed in this study are summarized in Table II. Ripples on the bead surface occur corresponding to the pulsing period. The ripple shape changes depending on pulse frequency. With high frequency and fast travel speed, instead of the ripple effect disappearing, a humping phenomenon appears on the surface.

The most pronounced solidification pattern produced by penetration is a wavy shape, which is only at a pulse frequency of 0.5 Hz and a fast travel speed. Under other conditions, the solidification pattern is a straight line and no scalloping is present.

In the bead formation at extremely low frequency, the melt width and the melt penetration depth increase, which is a result of perfect correspondence to the pulse current. At high frequency, the surface melt is fluctuated and agitated by the pulsed current arc without corresponding to the pulse period, which causes discontinuous bead formation.

A minimum grain size was obtained at pulse frequencies of 50 and 100 Hz and with faster travel speed. Thus, a most significant decrease in the grain size appeared to be achieved in both the fusion and heat-affected zones. However, because at such faster travel

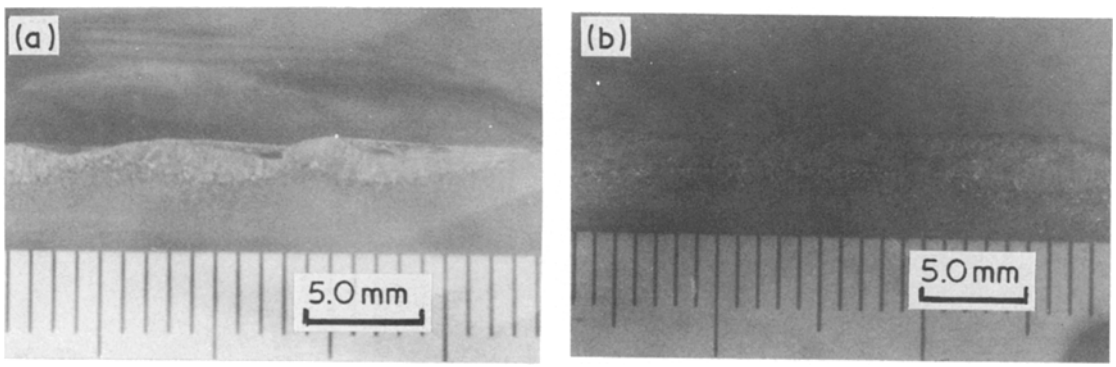

Figure 14 Macro longitudinal cross-sections of the mild steel surface beads. Pulse current 250 A, base current 150 A, pulse frequency 0.5 Hz, pulse time ratio 50%. (a) Wavy, travel speed 280 mm min^{-1}; (b) waveless, travel speed 130 mm min^{-1}.

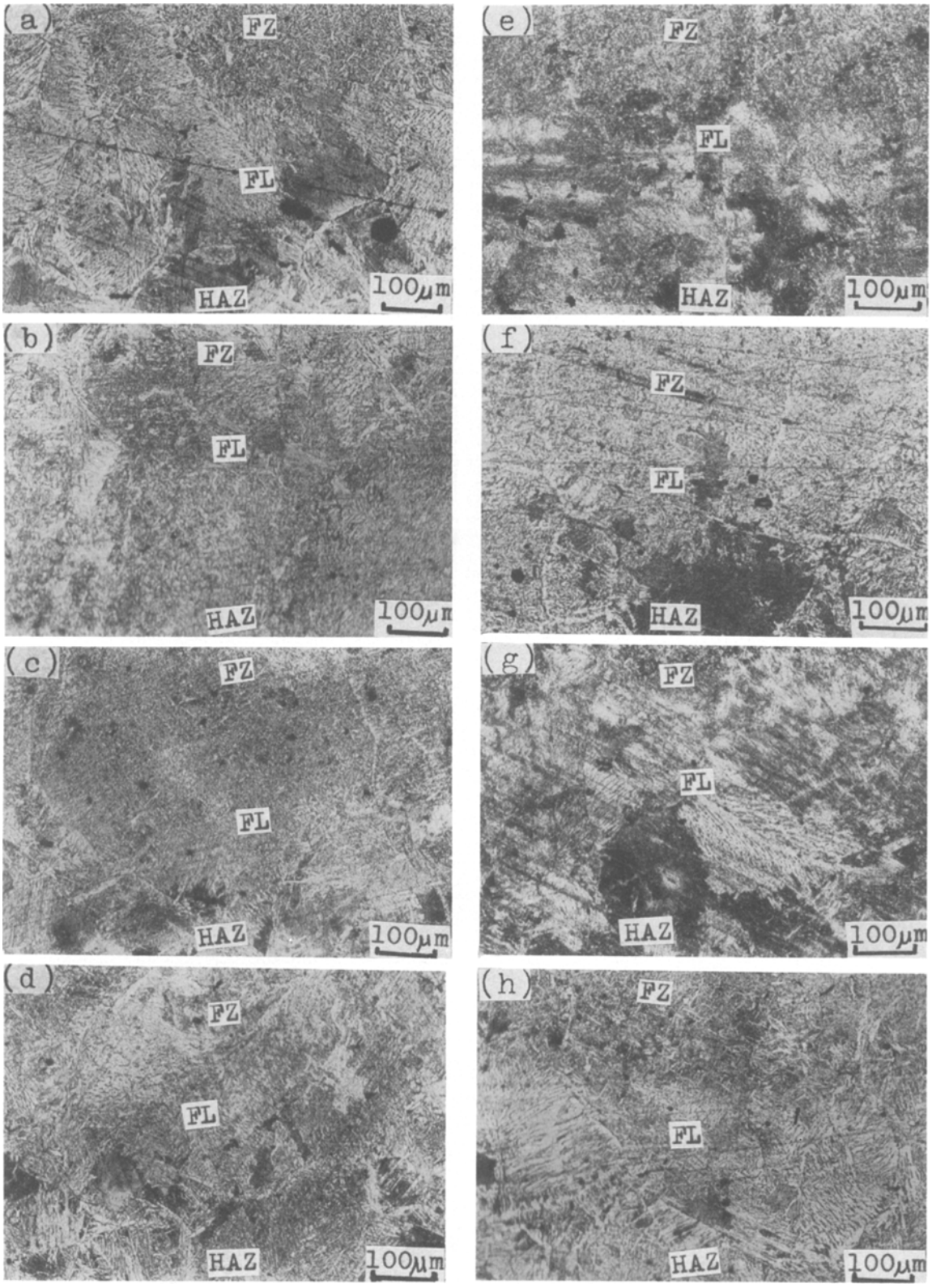

Figure 15 Longitudinal microstructures of mild steel for a travel speed of 130 mm min^{-1} with various pulse frequencies. Pulse current 250 A, base current 150 A, pulse time ratio 50%. (a) 0.45 Hz, (b) 1.0 Hz, (c) 2.5 Hz, (d) 5.0 Hz, (e) 50 Hz, (f) 100 Hz, (g) 200 Hz, (h) 500 Hz.

speed and pulse frequencies, the bead appearance is very poor, it is not available for consideration of pertinent bead formation. From the viewpoint of both morphology of bead formation and microstructure of fusion-boundary region, it became evident that the best bead was obtained at frequencies of 2.5 and 5.0 Hz, and a travel speed of 280 mm min^{-1}, as shown in Fig. 8 and Table II. In such a case, a favourable and gradual change from columnar to equiaxed grain structure occurs metallographically. Thus, a perfect bead and a significant reduction in grain size is possible by valid choice of pulsed current arc parameters.

4. Conclusions

The influence of pulse frequency on surface bead formation and the fusion-boundary microstructure of a mild steel was investigated by using pulsed current TIG arc in the low (0.5 to 5.0 Hz) and middle (50 to

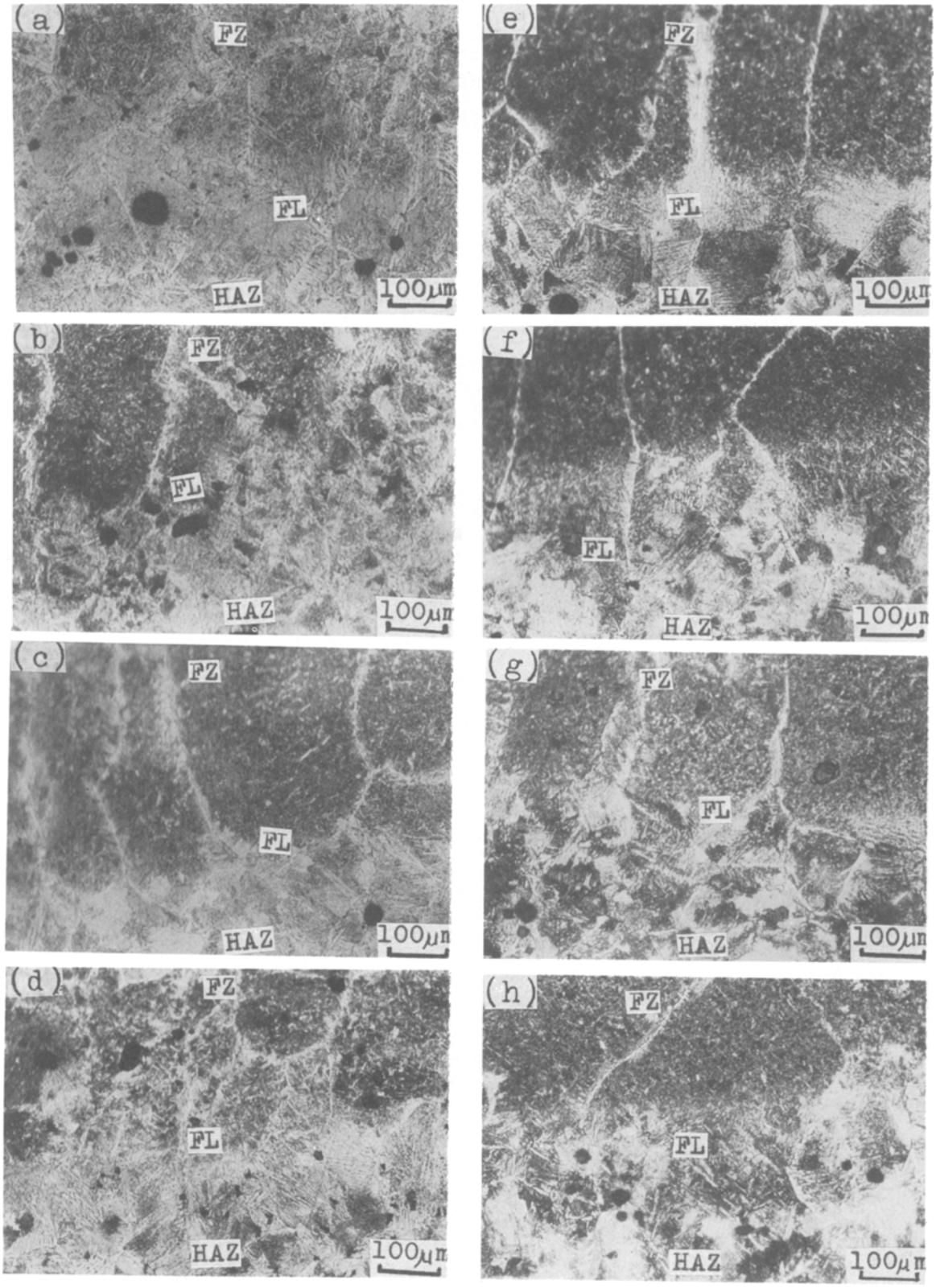

Figure 16 Longitudinal microstructures of mild steel for a travel speed of 280 mm min^{-1} with various pulse frequencies. Pulse current 250 A, base current 150 A, pulse time ratio 50%. (a) 0.5 Hz, (b) 1.0 Hz, (c) 2.5 Hz, (d) 5.0 Hz, (e) 50 Hz, (f) 100 Hz, (g) 200 Hz, (g) 500 Hz.

500 Hz) frequency regions. The principal results obtained are summarized below.

1. Surface bead width increases and decreases with increasing base current and travel speed of the torch, respectively.

2. The surface appearance shows a distinct ripple wave shape for the low frequency region, a small ripple wave shape for the middle frequency region with lower travel speed, and a humped bead shape for for the middle frequency region with faster travel speed.

3. The number of ripples produced on the surface bead increases parabolically with increasing pulse frequency and decreases with increasing travel speed. Increasing the pulse frequency seems to hold the ripple number constant, but, as the travel speed becomes fast, the number of ripples cannot be counted.

4. Bead width and depth decrease with increasing

TABLE II Morphology of mild steel bead formation on the bead appearance and microstructure of the fusion-boundary region with various pulse frequencies under a pulsed current arc. Pulse current = 250 A, base current = 150 A, pulse time ratio = 50%

Pulse frequency (Hz)	Travel speed 130 mm min^{-1}				Travel speed 280 mm min^{-1}			
	Bead appearance	Microstructure			Bead appearance	Microstructure		
		FZ	FL	HAZ		FZ	FL	HAZ
Low								
0.5	Ripples	Columnar	Smooth	Primary ferrite	Large ripples	Columnar	Distinct	Ferrite side plates
1.0	Ripples	Columnar	Smooth	Primary ferrite	Large ripples	Columnar	More distinct	Ferrite side plates
2.5	Small ripples	Equiaxed	Smooth	Ferrite side plates, fine pearlites	Small ripples	Equiaxed, fine pearlite	Most distinct	Acicular ferrites, fine pearlite
5.0	Very small ripples	Equiaxed	Distinct	Ferrite side plates, fine pearlites	Small ripples	Equiaxed, fine pearlite	Most distinct	Acicular ferrites, fine pearlites
Middle								
50	Very small ripples	Equiaxed	Distinct	Ferrite side plates, fine pearlites	Humped bead	Equiaxed, very fine pearlite	Most distinct	Acicular ferrites, fine pearlites
100	Very small ripples	Equiaxed	Distinct	Ferrite side plates, fine pearlites	Humped bead	Equiaxed, very fine pearlite	Most distinct	Acicular ferrites, fine pearlites
200	Very small ripples	Columnar	Smooth	Primary ferrite	Humped bead	Columnar	Distinct	Ferrite side plates
500	Very small ripples	Columnar	Smooth	Primary ferrite	Very slender humped bead	Columnar	Distinct	Ferrite side plates

pulse frequency and travel speed. A large decrease in the penetration is recognized at middle frequencies, which is probably the result of a lowering of arc gouging and a discontinuity of the bead formed.

5. The minimum grain size was obtained at pulse frequencies of 2.5, 5.0, 50 and 100 Hz, which had an equiaxed grain structure in the fusion zone, and consisted of a ferrite side plate or acicular ferrite and fine pearlite in the HAZ.

6. It was found that the best bead was achieved at pulse frequencies of 2.5 and 5.0 Hz, and a travel speed of 280 mm min^{-1}.

Acknowledgement

The author thanks the Ministry of Education, Science and Culture for the Grant-in-Aid for Scientific Research, Japan.

References

1. W. TROYER, M. TOMSIC and R. BARHORST, *Weld. J.* **56** (1977) 26.
2. H. MARUO and Y. HIRATA, *Q. J. Jpn Weld. Soc.* **3** (1985) 253.
3. A. A. OMAR and C. D. LUNDIN, *Weld. J.* **58** (1979) 97s.
4. D. W. BECKER and C. M. ADAMS Jr, *ibid.* **58** (1979) 143s.
5. T. WATANABE, H. NAKAMURA and K. EI, *Q. J. Jpn Weld. Soc.* **5** (1987) 17.
6. G. M. ECER, *Weld. J.* **59** (1980) 183s.

Received 14 September
and accepted 10 December 1987